Advances in Environmental Research, *Vol. 12, No. 1 (2023) 17-40*
https://doi.org/10.12989/aer.2023.12.1.017

Regeneration and modeling of fixed-bed adsorption of fluoride on bone char

Hugo D. García[1a], Rigoberto Tovar[*1], Carlos J. Durán[2a], Virginia Hernández[1b], Ma. R. Moreno[1c] and Ma. A. Pérez[3a]

[1]TecNM/Instituto Tecnológico de Aguascalientes. C.P. 20256. México
[2]Universidad de Extremadura, ES-06006. Badajoz, Spain
[3]Facultad de Ciencias Químicas. Universidad Autónoma de Puebla. Apdo. Postal J-55. Puebla, Pue., México

(Received November 28, 2021, Revised February 20, 2023, Accepted February 23, 2023)

Abstract. This article presents studies of the adsorption process in a continuous system of fluoride solutions at a concentration of 30 mg/L using a bone char packed in fixed-bed columns, as well as regeneration studies in the same system using HNO_3, HCl and NaOH at 0.01, 0.1 and 1 M. The Thomas Model, Artificial Neural Networks (ANNs), Numerical Integration and Mass Transfer Zone were used for the modeling of asyemmetrical breakthrough curves obtained from the fluoride adsorption on bone char. The maximum adsorption capacity of the breakthrough curves was estimated, and various design parameters of the columns were obtained for the different operating conditions. Results showed that an improvement in the modeling capabilities of the Thomas model can be obtained using ANNs. Moreover, ANNs are useful for determining reasonable and accurate design parameters of packed-bed adsorption columns. This modeling approach can be useful for the process system engineering of dynamic adsorption systems involved in the field of water treatment and purification. It is important to highlight that the obtained results indicate that, when using HCl or HNO_3 at a concentration of 0.1 M, a large number of adsorption-desorption cycles are obtained and, therefore, the highest values of adsorption capacity, which leads to a reduction in operation costs.

Keywords: adsorption; bone char; fixed-bed; fluoride; modeling; regeneration

1. Introduction

Water pollution is currently a subject of great interest worldwide, since water contains a wide variety of organic and inorganic compounds. Respect to fluoride, the WHO recommends a concentration of 0.7 mg/L for drinking water, as the toxicity of this chemical element begins at 1 mg/L (Fawell *et al*. 2006). High concentrations of fluoride in drinking water are a problem that affects 23 countries, including Mexico (Susheela *et al*. 1992). As a special case, in the state of Aguascalientes, the sources of water supply have been studied, finding that 43.7% of these sources exceed the established concentration. Therefore, if the water ingested exceeds the recommended concentration, the human body is exposed to serious damage, such as dental and skeletal fluorosis, renal dysfunctions, gastrointestinal disorders and gastric irritations, among other affectations

*Corresponding author, Ph.D., E-mail: rigtogo@hotmail.com

http://www.techno-press.org/?journal=aer&subpage=7 ISSN: 2234-1722 (Print), 2234-1730 (Online)

(Susheela *et al*. 1992, Yiamouyiannis and Burk 1997, Díaz *et al*. 1997, Hernández *et al*. 2003).

Thus, numerous treatment techniques have been used with the aim of reducing the concentration of fluoride in aqueous effluents. Specifically, adsorption is effective, simple, cost effective and widely adaptable for different types of contaminants and fluids. Among the new adsorption materials are those of inorganic nature, such as alum, clays, iron oxides, oxides and magnesium compounds; on the other hand, there are also biomaterials, which include algae, fungi, cherry laurel seeds and biopolymers, such as chitin, and its derivative, chitosan (Choy *et al*. 2004, O´Conell *et al*. 2008, Öztürk *et al.* 2021, Singh *et al*. 2013, Zhu *et al.* 2017). However, among the range of adsorbents studied for the removal of fluoride from water, the most recommended in the literature are activated alumina and bone char, due to their high adsorption capacity (Das *et al*. 2005).

Specifically, the use of bone char in the adsorption of fluorides from solutions and well water has been reported to compare its performance. For example, a bone char was used for the removal of fluorides from water in a well in San Luis Potosí, Mexico; in which anions such as Cl^-, NO_2^-, NO_3^-, CO_3^{2-}, HCO_3^-, SO_4^{2-} were found. Of these, the main competitor was the Cl^-; however, it was observed that the affinity of F^- towards bone char is much higher than that of Cl^-; therefore, F^- ions do not compete against Cl^- ions for the active sites on bone char. Specifically, the affinity in this adsorbent was: $F^- > Cl^- > CO_3^{2-} > NO_3^- > HCO_3^- > SO_4^{2-}$ (Leyva *et al.* 2010). Also, studies have been carried out in Aguascalientes, Mexico, due to high concentrations of fluorides in drinking water using a bone char. They conclude that the concentrations of the various ions present in said water do not directly interfere with the removal of fluorides (Rojas *et al*. 2013). Finally, my PhD student carried out adsorption studies using well water and precisely the bone char used in this paper. When comparing the adsorption capacities obtained with fluoride solution and well water from Aguascalientes, Mexico, it was observed that it is similar in both cases, with which it can be concluded that anions such as Cl^-, NO_3^-, HCO_3^-, SO_4^{2-} , PO_4^{3-}, CO_3^{2-}, among others, which are present in well water, have a negligible or no interaction effect for fluorides in the adsorption process.

Systems for removing fluorides from water usually employ the configuration of packed-bed columns. This system is very flexible and easy in terms of design and operation, and it offers several advantages, such as: 1) the effective contact between the adsorbent and the fluid to be treated, 2) the improved adsorption rates due to the fact that the adsorbent is continuously in contact with a fresh solution, 3) the feasibility of large-scale water treatment in a short time, 4) the possibility of performing the adsorbent regeneration in the same column, and 5) the low-moderate cost of the equipment and supplies required for the column operation (Dubey *et al.* 2021, Millar *et al.* 2017, Oguz and Ersoy 2010).

With respect to the regeneration of these adsorbents, as is mentioned above, one of the challenges that researchers face is both the mitigation of fluoride contamination and the generation of waste used in the removal of these contaminants, since, in most cases, the final disposal of said residues is unknown. In view of this, different methods of physical modification have been developed, such as treatments with microwaves, ozone and plasma, as well as methods of chemical modification, such as treatments with acids and bases, among others (Bhatnagar *et al*. 2013, Gupta *et al*. 2007, Louadj *et al.* 2021). The studies reported in the literature on the regeneration of adsorbents are limited, since this process is rare or is used directly in the activation of carbons. In this sense, it should be noted that desorption, as a regenerative process, cannot only cause an increase in the total adsorption capacity when reusing the adsorbent in a subsequent process of removal of the contaminant, but it can also modify the surface of the bone char. In this study, we

propose desorption, or regeneration, as an alternative that can reduce the costs in the use of adsorbents and increase the cycles of use in the removal of contaminants, in this specific case, for the removal of fluoride present in water.

Modelling of experimental data from adsorption processes is a very important means of predicting the mechanisms of various adsorption systems, such is the case of the applications of adsorption isotherms, the use of linear regression analysis, nonlinear regression analysis, and error functions for optimum adsorption data analysis (Ayawei *et al*. 2017). For example, Hosseine and Denayer (2022), reviewed the progresses made in implementation of mathematical modeling, simulation and optimization methods for biogas upgrading with emphasis on adsorption based processes. Firstly, the significance of biogas upgrading and the role of computational methods are explained. Then, strategies and methodologies for development of mathematical models and process simulations based on the governing transport mechanisms are described considering pressure swing adsorption, vacuum pressure swing adsorption, temperature swing adsorption and fixed adsorption beds for trace removal. For instance, an author introduced a generic modeling framework for modeling gas separation in multi-bed PSA units (Pressure Swing Adsorption). In the proposed framework, they considered various transport mechanisms with defined boundary conditions and operating procedures. All the equations were implemented in general PROcess Modelling System (gPROMS) environment. Another author modeled each fixed bed as a nonlinear distributed parameter system and then used a non-linear feedforward and a linear feedback schemes to control the process parameters such as product purity. Another author carried out an extensive study on modeling and simulation of adsorptive H_2S removal from biogas; the dynamic behavior of the process was studied using two distinct approaches: one using Bohart–Adams model relying on the rectangular isotherm particular to the processes involving chemical reactions. Another approach was based on the LDF model solved both analytically and numerically using Klinkenberg equation and in Aspen Adsorption, respectively. The quantitative characterisation of the performance of packed-bed adsorption columns involves the modeling and prediction of the breakthrough curve. This modeling stage is fundamental for the design and optimisation of this separation system. In fact, extensive studies at a pilot plant scale can be avoided if the breakthrough curves for adsorption columns can be reliably predicted using laboratory measurements (Ghorai and Pant 2005). The modelling of packed-bed adsorption processes using a theoretical and rigorous model usually requires the application of numerical methods, which may show convergence problems due to poor initialisation and non-linearity of the problem to be solved. For example, different models (e.g., Bohart–Adams, Thomas, Yoon–Nelson, Clark and the error-function model) are suitable for the data correlation of symmetrical breakthrough curves, although they may be inadequate and fail to describe the performance of packed-bed columns with a complex adsorption process (i.e., asyemmetrical breakthrough curves). Currently, several mathematical models have been used to describe the adsorption of single-component solutions in fixed-bed packed columns (Gong *et al.* 2014, Yu *et al*. 2014, Hernández-Eudave *et al*. 2015, Kyzas *et al*. 2015), among which are mentioned: the Thomas model, Yoon-Nelson, Clark, Bohart-Adams, Yan, BDST (Bed Depth Service Time). For example: Han *et al.* (2007) applied the Thomas model in its linear and non-linear form in continuous system adsorption studies using zeolites as adsorbent. Similarly, Han *et al.* 2009 used the Thomas, Bohart-Adams, Yoon-Nelson, Clark and BDST models in order to predict the behavior of the breakthrough curves obtained in the adsorption studies of the MB dye using tree leaf powder. Kalavathy *et al.* (2010) used the Thomas and Boharts-Adams models to determine the behavior of heavy metal adsorption in fixed-bed columns packed with activated carbon prepared from sawdust. Gong *et al.* (2014) predicted

the behavior of the breakthrough curves with the Thomas, Boharts-Adams and Yoon-Nelson adsorption models during the continuous adsorption process of the methylene blue dye and Pb (II), using sand coated with graphite oxide. Kyzas *et al*. (2015) used the empirical model of Thomas, Yoon-Nelson and Bohart-Adams on the simultaneous adsorption of the heavy metal zinc and the cationic remazol red dye on grafted chitosan. Patel and Vashi in 2015 studied the model of Thomas, Yoon-Nelson and BDST to describe the behavior of the fixed-bed packed column using different natural adsorbents (neem leaf, guava and tamarind seed powder) for the removal dye from textile wastewater. Finally, Omidvar Borna in 2016 investigated the Thomas, Yoon-Nelson and Bohart-Adams model to analyze the behavior of the breakthrough curves in the Cr^{6+} adsorption. It is convenient to remark that the modeling of breakthrough curves is challenging due to the nonlinearity of equations used to describe the equilibrium, kinetics and mass transport phenomena involved in dynamic adsorption processes (Bravo *et al*. 2002). This study proposes an ANNs approach for the modeling of asyemmetrical adsorption breakthrough curves. Specifically, ANNs are used to improve the modeling capabilities of traditional breakthrough equations for adsorption systems involving priority water pollutants. The literature indicates that ANNs have been widely used to model complex relationships between inputs and outputs or to find patterns in selected data. For the case of dynamic adsorption systems, some studies have reported the application of ANNs as a black-box model (i.e., an empirical model that relies on measurements only) for data fitting of breakthrough curves (Texier *et al*. 2002, Cavas *et al*. 2011, Oguz and Ersoy 2010). In this study, several models were used to model the performance of packed-bed adsorption columns for the removal of fluoride from water using bone char. Furthermore, we report the desorption curves and the desorbed amount of fluoride in every desorption cycle. Finally, the proposed approach can be useful for the process system engineering of dynamic adsorption systems involved in the field of water treatment and purification.

2. Experimental methodology

2.1 Bone char used in adsorption experiments

The Fluoride adsorption experiments were performed using a commercial bone char from Mexico (BCM). Table 1 provides the general specifications of this adsorbent provided by the supplier. This adsorbent was selected because the hydroxyapatite, with chemical structure $Ca_{10}(PO_4)_6(OH)_2$, is the principal component of bone chars according to results reported in the literature (Tovar *et al*. 2013); and these hydroxyl groups are involved in the fluoride removal by ion exchange. Physicochemical properties and textural parameters of this adsorbent were determined in this study. Specifically, the elemental composition of bone char was determined with a LECO CHNS-932 elemental analyser and the oxygen content with a LECO VTF-900. Textural parameters were calculated from the nitrogen adsorption isotherms at 77 K, which were obtained with a Micromeritics TriStar II 3020. Organic functional groups were identified by FT-IR spectroscopy using a Thermo Nicolet 6700 spectrophotometer and the diffraction patterns of this adsorbent were recorded in a Bruker D8 Advance diffractometer equipped with a Cu Kα X-ray source operated at 40 kV and 40 mA. A single Göbel mirror configuration was used to monochromatise and focus the X-rays on the samples, attaining a highly efficient parallel beam geometry. Step scanning, with a step size of 0.02° 2θ and a scan step time of 5 s, was used to collect the diffraction data. Additionally, the physical morphology of bone char was observed

Table 1 Supplier specifications of bone char used in packed-bed adsorption columns for fluoride removal

Property[a]	BCM
Carbon content	10-15%
Tricalcium phosphate	80-85%
Specific surface area	104 m^2/g
Humidity	<4%

using a FE-SEM system (Quanta FEG 650, FEI) equipped with an EDX analyser (Ametek-EDAX). Adsorbent particles were dispersed on a graphite adhesive tab placed on an aluminum stub and no further coating was required. A semi-quantitative analysis of the inorganic elements was obtained by EDX and an average of three punctual analyses on the bone char surface at 20 µm was reported.

2.2 Fluoride adsorption experiments in packed-bed columns using BCM

Dynamic adsorption experiments were performed in a Pyrex glass column (internal diameter: 2.5 cm; length: 13 cm). This column was packed with 27 g (i.e., 7.5 cm of packing height) of the commercial bone char (particle size: 18–20 mesh fraction) and the bed porosity ranged from 25% to 30% for the adsorbent in all adsorption experiments. Fluoride breakthrough curves were obtained using the bone char, a feed fluoride concentration of 30 mg/L and a feed flow rate of 3.3 mL/min. These pollutant concentrations were selected based on the fact that the groundwater extracted in several regions of Mexico and other countries may show fluoride concentrations of up to 30 mg/L and higher (Susheela *et al.* 1992, Hernández *et al.* 2003, Singh *et al.* 2013). The feed flow rate corresponds to ~3.0 min of residence time, which is common in the use of packed-bed adsorption columns (Faur *et al.* 2008, Aguayo *et al.* 2011). Our experience in adsorption process regarding dynamic conditions indicates that residence times higher than 3 min do not significantly improve the removal process performance due to limitations caused by mass transfer phenomena. Fluoride solutions were prepared using analytical grade sodium fluoride (NaF) and deionised water. All adsorption experiments were performed at pH 7 and 30 ℃ using a peristaltic pump and an up-flow operation mode, which was used to avoid excessive head-loss and channelling. Several effluent samples were collected from the packed-bed column at regular time intervals and the fluoride concentration in all samples was determined to obtain the breakthrough curve. Fluoride concentrations were quantified using a fluoride ion selective electrode (Denver Instruments, UP-25) and TISAB buffer (Hach®) following the methodology described in the Standard Methods of Examination of Water and Wastewater. A linear calibration curve was used to determine the fluoride concentration in all samples.

2.3 Analysis and modelling of the breakthrough curves of fluoride adsorption on BCM

2.3.1 Calculation of design parameters of breakthrough curves

Design parameters of the packed-bed columns were calculated from the experimental data of the fluoride breakthrough curves using the bone char. Specifically, the mass transfer zone (*MTZ*) was calculated for different operating conditions of packed-bed columns using the next expression

$$MTZ = L\left(\frac{t_e - t_b}{t_e}\right) \quad (1)$$

where t_b is the breakthrough time, t_e is the exhaustion time and L is the bed height in cm. For this analysis, t_b was defined as the time when $[F^-]/[F^-]_0$=0.05, while t_e corresponds to $[F^-]/[F^-]_0$=0.95, where $[F^-]$ is the effluent fluoride concentration and $[F^-]_0$ is the feed fluoride concentration (both in mg/L). The overall adsorption zone (Δt) was also determined using

$$\Delta t = t_e - t_b \tag{2}$$

The retardation factor (r_f) was used to determine the rate at which the pollutant moves within the packed-bed column (Apiratikul and Pavasant 2008). This parameter was obtained from the treated volume per void volume that gives $[F^-]/[F^-]_0$=0.5 or, equivalently, the operating time ($t_{50\%}$) of the packed-bed column when the effluent concentration has reached 50% of the influent concentration, thus

$$r_f = \frac{V_{50\%}}{AL\varepsilon} \tag{3}$$

where ε is the void volume of the packed-bed column, A is the cross sectional area of the column and L is the bed height of the column, respectively. Retardation factors were estimated for all operating conditions used in the fluoride adsorption experiments. Finally, the bed adsorption capacity (q_{bed}) and the maximum adsorption capacity obtained from fluoride adsorption isotherms ($q_{e,max}$) were used to estimate the filter material usage rate (F_q)

$$F_q = \frac{q_{bed}}{q_{e,max}} \tag{4}$$

where q_{bed} and $q_{e,max}$ are given in mg/g and are obtained at the same conditions of temperature and pH. Note that q_{bed} can be calculated via the integration of the experimental data $\frac{[F^-]_t}{[F^-]_0}$ versus t, or using a specific breakthrough equation (e.g., Thomas model). All these design parameters were used to characterise the performance of the bone char in fluoride adsorption columns at different operating conditions.

2.3.2 Data fitting of fluoride breakthrough curves using Thomas model

The Thomas model (Thomas 1944) was used to model the fluoride adsorption breakthrough curves using BCM. This breakthrough model is based on Langmuir-type adsorption– desorption and assumes isothermal and isobaric operating conditions and a constant column void fraction; the radial and axial dispersions are negligible in the packed-bed column. For the case of fluoride adsorption, this model is given by

$$\frac{[F^-]_t}{[F^-]_0} = \frac{1}{1+\exp\left(\frac{k_{Th}}{Q}\left(q_{bed,T}W_{bed} - [F^-]_0 V_{eff}\right)\right)} \tag{5}$$

where V_{eff} is the treated volume of fluoride solution in L, Q is the feed flow rate (given in L/h), W_{bed} is the amount of bone char packed in the columns (given in g), $q_{bed,T}$ is the adsorption capacity of the packed-bed column estimated by the model (given in mg/g) and k_{Th} is the Thomas rate constant (given in L/h mg). Parameters k_{Th} and $q_{bed,T}$ can be obtained from a linear regression approach using the following linearised form of the Thomas model

$$ln\left(\frac{[F^-]_0}{[F^-]_t} - 1\right) = \frac{k_{Th}q_{bed,T}W_{bed}}{Q} - \frac{k_{Th}[F^-]_0 V_{eff}}{Q} \tag{6}$$

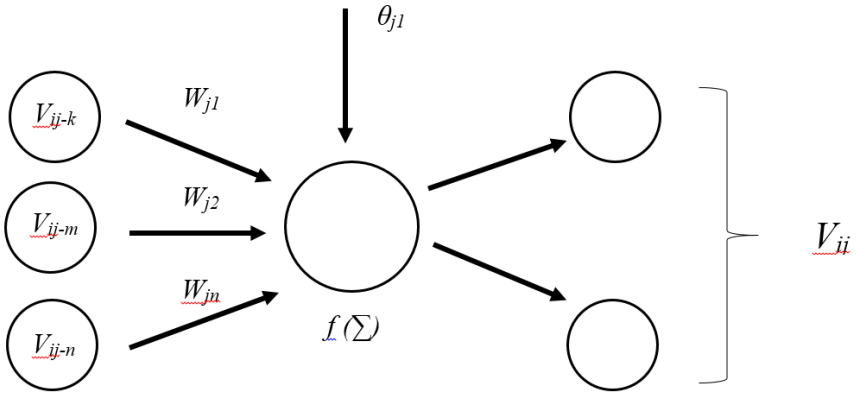

Fig. 1 Illustration of a neuron in an ANN model

A plot of $ln\left(\frac{[F^-]_0}{[F^-]_t}-1\right)$ versus t at the given operating conditions (i.e., feed flow rate, temperature and pH) is used for this linear regression. The Statistica software was used to perform the linear regression of the Thomas model using the fluoride breakthrough curves of the tested bone char.

2.3.3 ANNs for data fitting of breakthrough curves

As was previously stated, the linear regression approach is extensively used for determining the parameters of the Thomas model and other traditional breakthrough equations. However, this approach may fail to fit the experimental adsorption data of asyemmetrical breakthrough curves. In fact, our experience and results of other studies on adsorption processes for water treatment indicate that the experimental breakthrough curves obtained for the removal of fluorides and other priority pollutants (e.g., heavy metals, dyes) are commonly asyemmetrical, e.g., (Aguayo *et al.* 2011, Cavas *et al.* 2011, Oguz and Ersoy 2010). Based on this fact, we used ANNs to model the breakthrough curves. It is important to remark that some authors have used ANNs for modelling adsorption breakthrough curves (Cavas *et al.* 2011, Oguz and Ersoy 2010). ANNs are black-box (i.e., empirical) computational models inspired by biological neural networks. ANNs can predict the performance of complex and non-linear problems and find patterns in data analysis relying only on measurements (inputs and outputs) (Basheer and Hajmeer 2000). A neural network consists of input, hidden and output layers, which are constituted by an interconnected group of artificial neurons. These artificial neurons are interconnected to each other via connection weights, which represent the relative strength of an input neuron in contributing to the output neuron, see Fig. 1. Formally, the net input Y_{ij} of the neuron j in the layer i is given by

$$Y_{ij=}\sum_{k=1}^{n_{i-1}} w_{ijk}V_{i-1,k}+\theta_{ij} \quad (7)$$

$$V_{ij}=g(Y_{ij}) \quad (8)$$

where w_{ijk} is the connection weight, V_{ik} is the neuron input and θ_{ij} is the neuron bias. An activation function $g(Y_{ij})$ is used to calculate the neuron output V_{ij} given the set of neuron inputs. The most common activation function is the sigmoid function, which was used in this study for the neurons

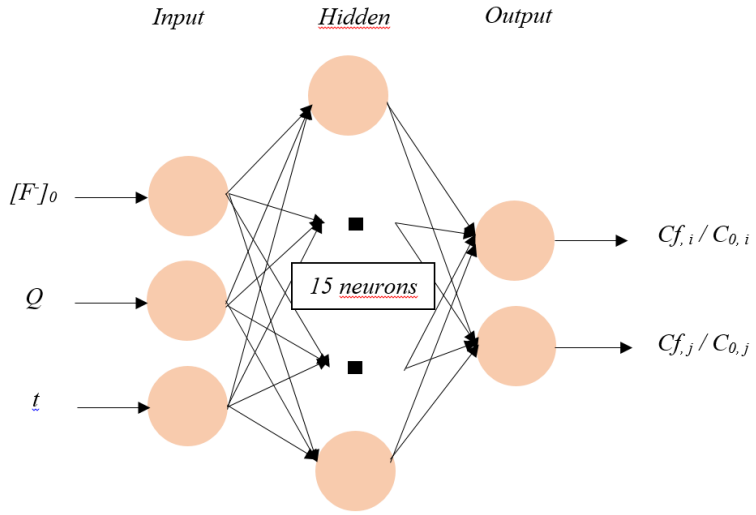

Fig. 2 Artificial neural network architecture used for modelling the fluoride adsorption breakthrough curve using BCM

of hidden layers, while an identity function (i.e., $V_{ij} = Y_{ij}$) was used in the output layer. A training process was used to determine suitable values of w and θ for each neuron of the ANNs model. This training was performed using input data and target output values obtained from the studied system. Thus, we used the classical backpropagation algorithm for ANNs training, which is a first-order gradient descent method.

In this study, a model using a feed-forward ANNs architecture was proposed for data fitting of fluoride breakthrough curves (see Fig. 2). Prior to the ANNs training process, the values of input neurons were normalised. Parameters of the Thomas model, which were used to calculate the values of $\frac{[F^-]_t}{[F^-]_0}$, were considered as the targets of the ANNs model subject to the non-negativity restrictions: $k_{Th} > 0$ and $q_{bed,T} > 0$. These restrictions were considered for the model based on the fact that both parameters of the Thomas equation have a physical and theoretical meaning. Without these restrictions, the model may find negative values for these model parameters, thus losing its physical significance. The training of the model was performed via the minimisation of the following objective function

$$F_{obj} = \frac{1}{2}\sum_{m=1}^{n_n}\sum_{j=1}^{ndat}\left(\frac{[F^-]_t^{exp}}{[F^-]_0} - \frac{[F^-]_t^{calc}}{[F^-]_0}\right)^2 \quad (9)$$

where n_{dat} is the number of experimental data used for the training of the model, n_n is the number of output neurons and superscripts *calc* and *exp* indicate the calculated and experimental values, respectively. The MATLAB® software was used for the data modelling of fluoride breakthrough curves using this model based on ANNs and Thomas equation.

For ANNs training, the input data included the feed fluoride concentration ($[F^-]_0$), the operation time of packed-bed column (t) and the feed flow (Q) obtained from fluoride breakthrough curves. Previous studies have used these input variables for the modelling of breakthrough curves using black-box ANNs models (Cavas *et al.* 2011, Oguz and Ersoy 2010), since they have a statistical influence on the performance of dynamic adsorption processes. Additionally, this set of input

variables is uncorrelated, which is in agreement with the basis of the principal component analysis approach. The architecture of the ANN model was determined based on preliminary calculations using a trial and error procedure, where the combination of input variables and the number of hidden layers and neurons were modified until finding a proper ANN architecture. Several ANN models were analysed and they included different configurations of the input variables, i.e.: $t - Q$, $t - [F^-]_0$, $[F^-]_0 - Q$ *and* $t - Q - [F^-]_0$, where the ANN model with three input variables offered the best performance. The results of the sensitivity analysis indicated the following trend for the most influential variables: t > $[F^-]_0$ > Q. Therefore, the ANNs architecture used for modelling the fluoride adsorption breakthrough curves consisted of an input layer with three neurons $t - Q - [F^-]_0$, two hidden layers with 15 neurons for each layer, and one output layer (see Fig. 2). It is convenient to remark that our calculations indicated that a high number of hidden neurons (i.e., >15) caused overfitting of the model. Finally, the results obtained from the linear regression approach and those obtained from the hybrid model were compared and analysed using statistical criteria and design parameter calculations of packed-bed columns.

2.3.4 Data fitting of fluoride breakthrough curves using numerical integration

The results obtained in the breakthrough curves were used to estimate the adsorption capacity of the packed beds. Numerical integration is a polynomial model adjusted individually to each breakthrough curve. The numerical integration of the following function was performed, which describes the material balance for the packed bed.

$$q_{bed} = \int_{t=0}^{t} (C_0 - C)\frac{Q}{M}\, dt \tag{10}$$

where q_{bed} is the adsorption capacity of the packed bed (given in mg/g), C_0 and C are the concentrations at the entrance and exit of the packed column, respectively (given in mg/L), Q is the volumetric flow (given in mL/min), and M is the mass of the packed bed (given in g). POLYMATH® was used for the modelling of numerical integration using the fluoride breakthrough curves of BCM.

2.4 Fluoride desorption experiments in packed-bed columns using BCM

At the end of each fluoride adsorption study, a desorption process, or regeneration, was carried out directly in the packed-bed columns. Fluoride desorption studies were carried out according to some conditions of an experimental design of a complete factorial 3^3, which was previously carried out in a batch system. The factors were: regenerant (factor A), regenerant concentration (factor B) and contact time (factor C). The regenerants used were HNO_3, HCl and NaOH, with concentrations of 0.01, 0.1 and 1 M, and contact time of 5, 60 and 120 minutes.

3. Results and discussion

3.1 Physicochemical and textural characterisation of bone char

It is important to analyse the composition of the BCM used in the fluoride removal studies. The results of elemental composition and the inorganic constituents identified by EDX in BCM are reported in Table 2.

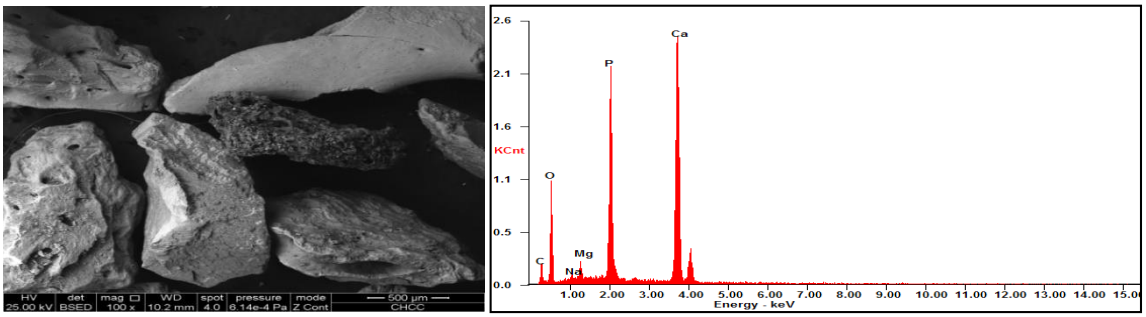

Fig. 3 SEM images and EDX results of BCM

Table 2 Results of ultimate analysis and principal elements identified by EDX in the BCM used for the fluoride removal from water

Ultimate analysis		EDX results [a]	
Element (w%)	BCM	Element (w%)	BCM
C	6.1	Mg	1.26
H	0.5	P	16.64
N	0.8	Ca	30.72
S	0.0		
O	10.3		

[a] Average of three determinations

In this case, it is important to highlight the percentage of carbon, hydrogen and oxygen. Specifically, BCM showed a high content of oxygen and hydrogen and, probably, this adsorbent may have a high quantity of hydroxyl groups. These hydroxyl groups are involved in the fluoride removal according to the following reaction (Rao *et al.* 2009)

$$Ca_{10}(PO_4)_6(OH)_2 + 2F^- \rightarrow Ca_{10}(PO_4)_6F_2 + 2OH^- \quad (14)$$

where $Ca_{10}(PO_4)_6(OH)_2$ is the chemical structure of hydroxyapatite, which is the principal component of bone chars according to results reported in the literature (Bennett and Abram 1957, Choy and McKay 2005, Rao *et al.* 2009). Our results corroborated that Ca and P are the principal inorganic elements identified in BCM according to EDX analysis (see Table 2 and Fig. 3). Moreover, the diffraction patterns of the crystalline form of hydroxyapatite were observed in the X-ray results of BCM (Fig. 4(a)). In general, the diffraction patterns of this adsorbent are very similar to those reported for other bone chars obtained from bovine bones (Choy and McKay 2005) and swine (Pan *et al.* 2009). On the other hand, some characteristic peaks of hydroxyapatite were identified in the FT-IR spectrum of BCM at 1030 and 600 cm^{-1}, which can be assigned to vibrations of stretching and bending of phosphate, respectively (Dimovic´ *et al.* 2009) (see Fig. 4(b)). Additionally, other peaks were identified and the signal around 3400 cm^{-1} can be attributed to the existence of hydroxyl groups, whereas the peaks at 1460 cm^{-1} can be assigned to C–O stretching vibrations of carboxyl groups (Tovar *et al.* 2013). Lastly, the BCM particles have an irregular form and few pores are observed on the char surface (see Fig. 3). This morphology is

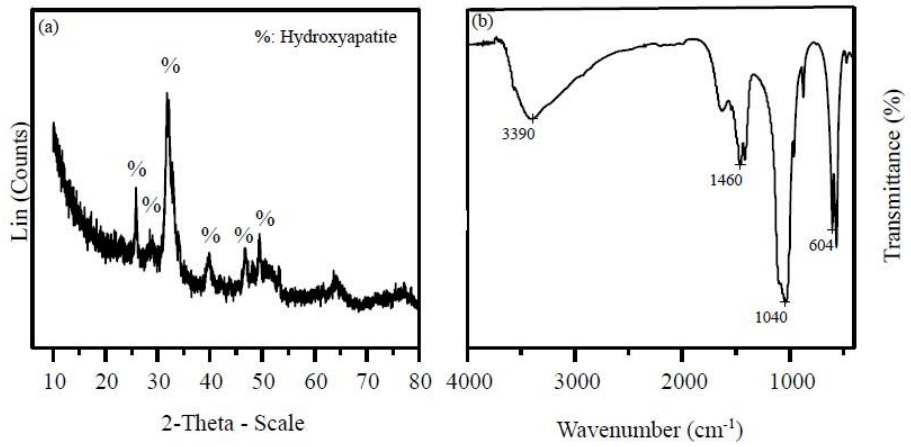

Fig. 4 (a) XRD patterns and (b) FT-IR spectra of BCM

associated with the low specific surface of this adsorbent, which was 104 m^2/g. These characterisation results are similar to those obtained for other commercial bone chars reported in the literature, such as those from Carvão Ativado do Brasil and Barnebey Sutclife Corporation (Hernández *et al.* 2007).

3.2 Breakthrough curves of fluoride adsorption using BCM

3.2.1 Adsorption studies of fluorides in a continuous system using HNO_3 as regenerant

Experimental data of fluoride breakthrough curves for BCM at different operating conditions of packed-bed columns are reported in Figs. 5-11. As expected, the characteristics and shape of fluoride breakthrough curves depend on the operating conditions of the adsorption columns (i.e., concentration and regenerant type). However, it is clear that all the fluoride breakthrough curves show a common S-shape, although they are asyemmetrical. All breakthrough curves obtained for BCM showed a slow approach of $C_f/C_0 \rightarrow 1.0$, which is a common characteristic of adsorption processes in a liquid phase, where the diffusion phenomena are the rate-limiting mass transport processes (Aksu and Gönen 2006).

In previous studies (Tovar *et al.* 2013), we reported the fluoride adsorption kinetics and isotherms obtained under batch conditions for BCM at 30℃ and pH 7. The results of fluoride adsorption kinetics were modelled using both pseudo first- and second-order kinetic models, and it was clear that the pseudo second-order model offers the best correlation for fluoride adsorption rates on BCM. On the other hand, fluoride adsorption isotherms were fitted to the Langmuir, Freundlich and Sips models. Both Langmuir and Sips are suitable for the correlation of fluoride adsorption isotherms on BCM. Based on this fact, we used the Langmuir isotherm model to determine the monolayer fluoride adsorption capacity (q_{max}): BCM: q_{max} = 4.51 mg/g. The results of fluoride breakthrough curves are consistent with the batch adsorption results and the monolayer adsorption capacity obtained from the Langmuir model, which indicate that BCM has the greatest fluoride adsorption capacity under both static and dynamic conditions. These maximum adsorption capacities from the Langmuir model were used to calculate the filter material usage rate (F_q) during the analysis of the design parameters of bone char packed-bed columns.

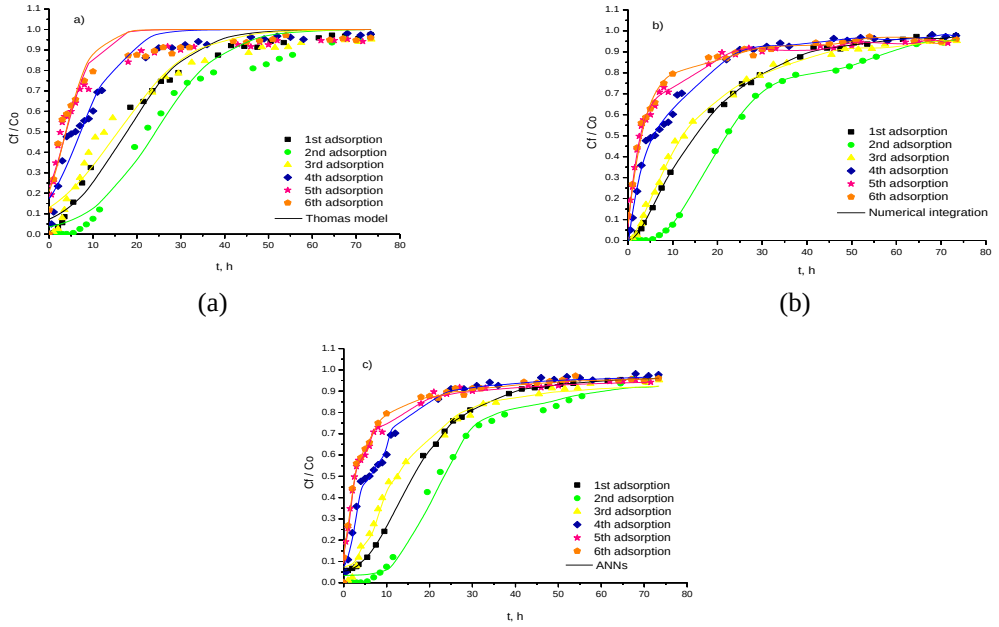

Fig. 5 Breakthrough curves of the fluoride adsorption-desorption process with HNO_3 0.1 M and their adjustment with: (a) Thomas model, (b) Numerical integration and (c) ANNs

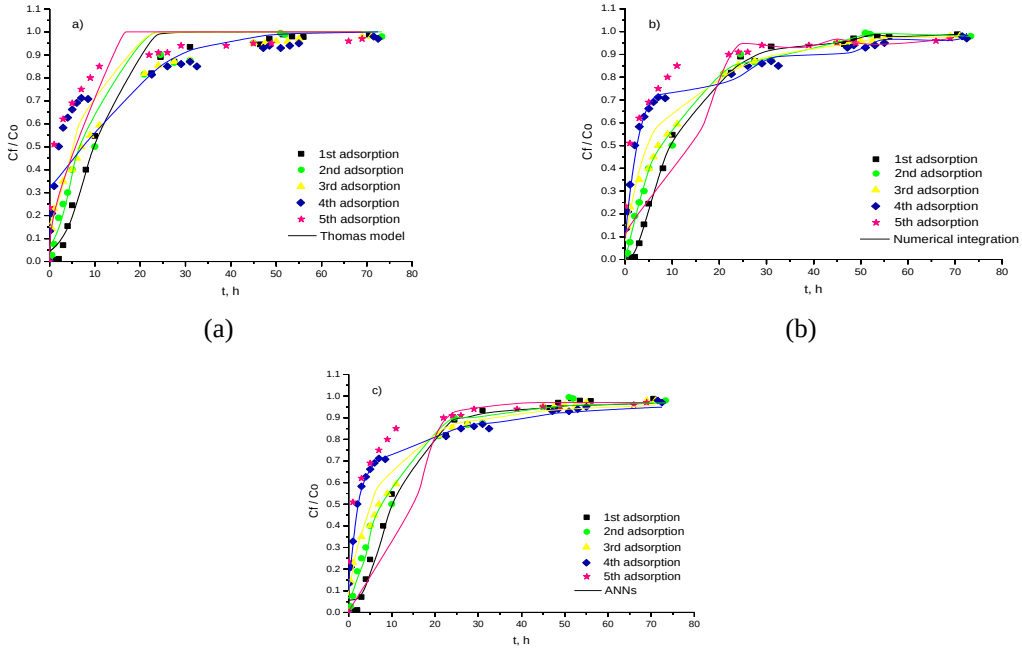

Fig. 6 Breakthrough curves of the fluoride adsorption-desorption process with HNO_3 0.01 M and their adjustment with: (a) Thomas model, (b) Numerical integration and (c) ANNs

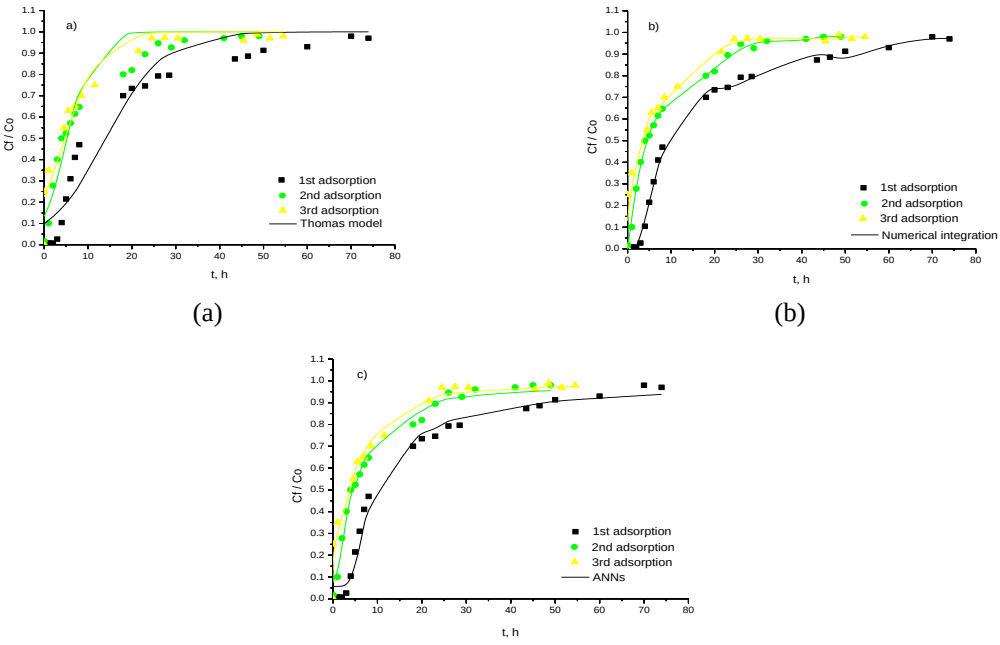

Fig. 7 Breakthrough curves of the fluoride adsorption-desorption process with HNO_3 1 M and their adjustment with: (a) Thomas model, (b) Numerical integration and (c) ANNs

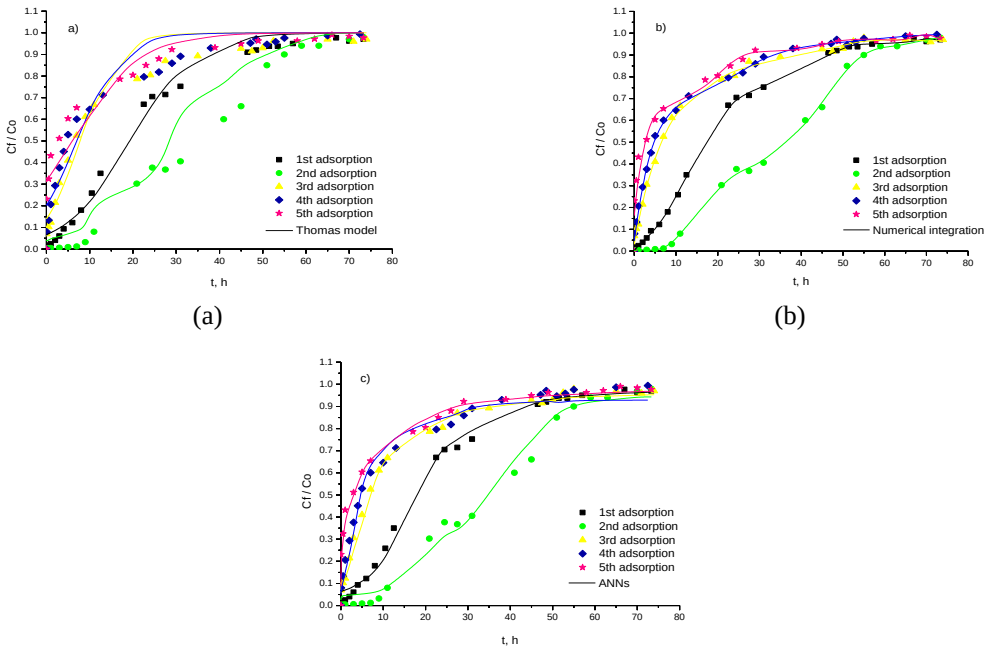

Fig. 8 Breakthrough curves of the fluoride adsorption-desorption process with HCl 0.1 M, and their adjustment with: (a) Thomas model, (b) Numerical integration and (c) ANNs

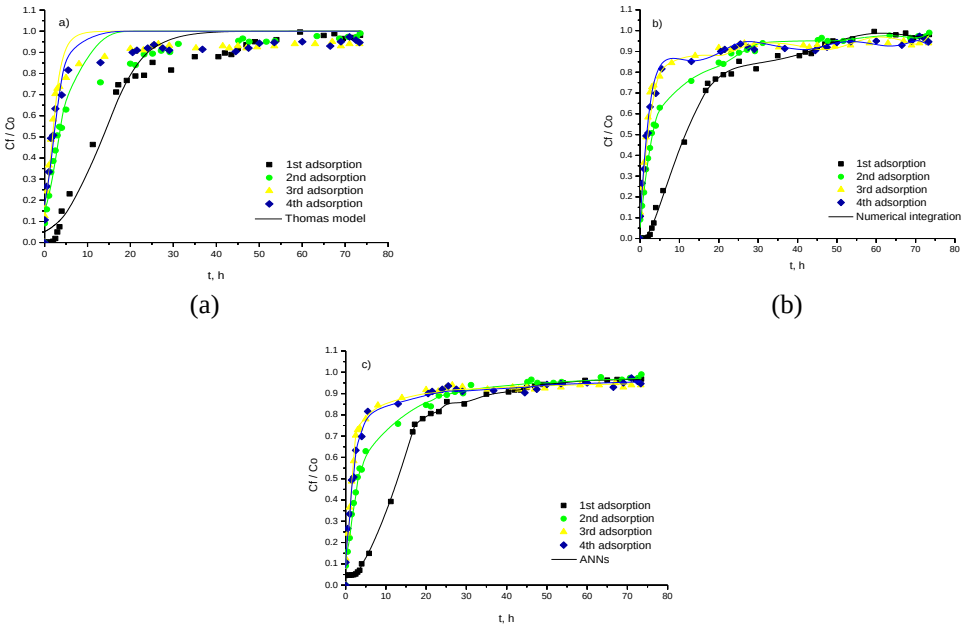

Fig. 9 Breakthrough curves of the fluoride adsorption-desorption process with HCl 0.01 M and their adjustment with: (a) Thomas model, (b) Numerical integration and (c) ANNs

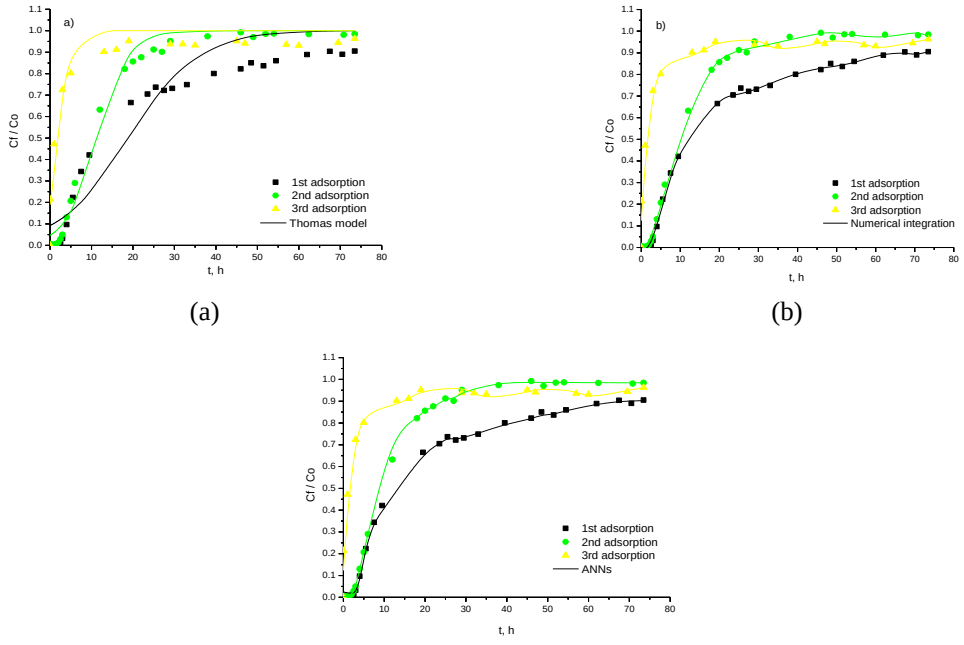

Fig. 10 Breakthrough curves of the fluoride adsorption-desorption process with HCl 1 M and their adjustment with: (a) Thomas model, (b) Numerical integration and (c) ANNs

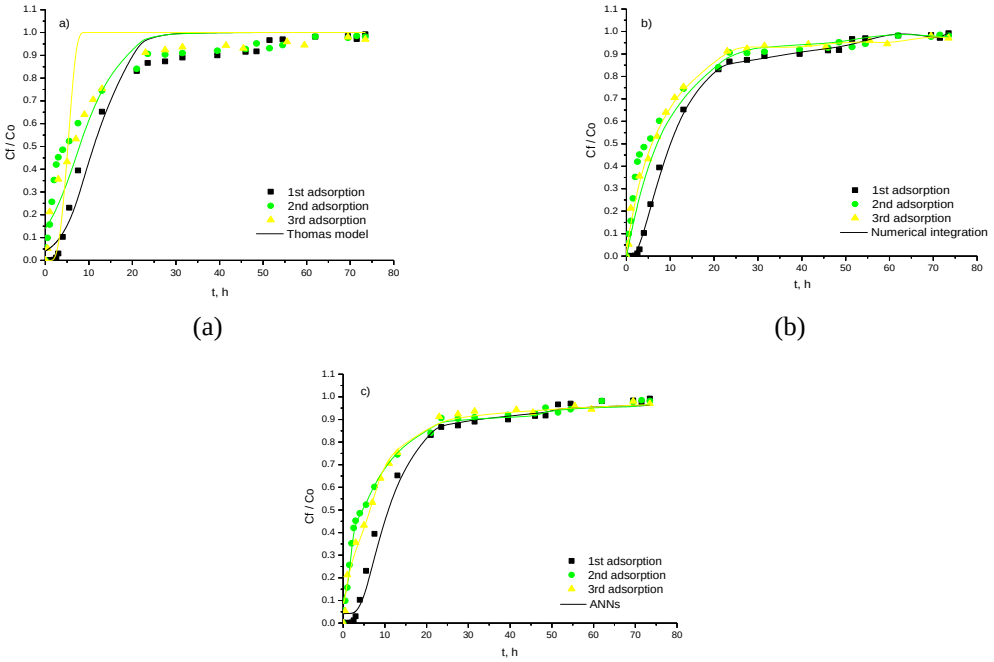

Fig. 11 Breakthrough curves of the fluoride adsorption-desorption process with NaOH 0.1 M and its adjustment with: (a) Thomas model, (b) Numerical integration and (c) ANNs

In preliminary adsorption-desorption studies carried out in our laboratory under the same conditions but in a batch system, it was determined that using HNO_3 at a concentration of 0.1 M, the best adsorption capacity results were obtained. Due to this, the first study in a continuous system shown in this article was using HNO_3 at that concentration. The number of adsorption-desorption cycles was determined according to the adsorption capacity obtained in each cycle, that is, in which cycle the adsorption capacity decreased drastically and/or remained almost constant. Therefore, the 6 adsorption-desorption cycles obtained for HNO_3 at 0.1 M were considered as a parameter to decide when to stop the other studies. However, to compare the regenerants and concentrations, only up to the third cycle was considered.

In Fig. 5, the breakthrough curve is first shown using the virgin adsorbent, i.e., used for the first time in fluoride adsorption. The breakthrough curve for the second adsorption shifts to the right with respect to the first adsorption, indicating an increase in fluoride adsorption capacity. Similar results were reported by Buamah *et al.* (2016). This increase may be due to the fact that the regenerant HNO_3 oxidizes BCM, forming OH^- groups on its surface, which causes an increase in ion exchange and, consequently, in the adsorption capacity of the adsorbent. This could also be due to the fact that, during the first desorption process with HNO_3 0.1 M, in addition to desorbing a large amount of fluoride, adsorbed in the first breakthrough curve, BCM increased its surface area, which was caused either by the removal of impurities (inorganic matter), the increase of total pore volume, or both. This assumption is based on the fact that HNO_3 is a chemical activator of bone chars and previous studies in the laboratory about the characterization of BCM modified with HNO_3 have shown a decrease in the ash content (from 50.25 to 15.70) and a large increase in its

surface area (from 104 to 895 m^2/g) and the total pore volume (0.209 to 1.005 cm^3/g). Furthermore, it has been reported that bone char contains hydroxyapatite. The latter compound has OH^- groups in its structure, which are the ones that interact with the fluorides in the solution; in other words, the ionic exchange between the two occurs during the adsorption process. By using HNO_3 during the regeneration process, which is a strong oxidant, it is generating more OH^- groups on the surface of BCM, increasing the interaction with fluorides, thereby favouring the removal of this pollutant. After the third breakthrough curve, they begin to move slowly to the left (*y-axis*), since, in each desorption cycle, BCM gradually loses its ability to adsorb fluorides, i.e., it does not fully regenerate.

Furthermore, Fig. 6 shows the fluoride breakthrough curves, although using HNO_3 at a concentration of 0.01 M as regenerant. The aim of these studies was to observe whether similar results were obtained at a lower HNO_3 concentration, in order to attain a reduction in operating costs. As can be seen, the behaviour is not similar to that obtained at 0.1 M HNO_3, i.e., in this case, the second breakthrough curve does not shift to the right, but slightly to the left with respect to the first curve, and so on. This may be due to the fact that, when using HNO_3 at a low concentration, only a small amount of the fluorides adsorbed in the previous stage are desorbed. Furthermore, it is not possible to generate a large quantity of OH^- groups on the surface of the carbon, limiting the increase of fluoride adsorption. This could also be due to the fact the surface area and total pore volume of BCM is not increased.

Lastly, adsorption-desorption studies were carried out using HNO_3 at a concentration of 1 M in order to analyse the possible increase in carbon yield with respect to the use of this regenerant at 0.1 and 0.01 M. Fig. 7 shows that the second breakthrough curve shifted largely toward the y-axis with respect to the first curve. Similarly, the third curve shifted to the left with respect to the second curve. This may be due to the fact that, when using such a high concentration of HNO_3, the regenerant-adsorbent contact was so aggressive that it caused the destruction of the structure of a large quantity of carbon, pulverizing it and reducing the carbon bed with the increasing desorption cycles, thus causing its rapid saturation.

3.2.2 Adsorption studies of fluorides in a continuous system using HCl as regenerant

In order to evaluate and compare the performance of the adsorbent with another type of regenerant, fluoride adsorption-desorption studies were carried out using HCl under the same conditions and concentrations of HNO_3, i.e., at 0.1, 0.01 and 1 M (see Figs. 8-10. As can be seen, the behaviour of the breakthrough curves is very similar to that obtained for HNO_3 at the same concentrations. For example, at 0.1 M, the second curve shifts to the right with respect to the first curve, indicating a considerable increase in adsorption capacity. This may be due to what was described above for HNO_3 at that concentration. Furthermore, when regenerating the adsorbent with HCl, active Cl^- sites are generated on its surface, which allows ion exchange with fluorides and consequently favours the removal of the contaminant (Hernández *et al*. 2013).

3.2.3 Adsorption studies of fluorides in a continuous system using NaOH as regenerant

NaOH was used as the third and last regenerant to be studied. The breakthrough curves using NaOH at 0.1 M are presented in Fig. 11. As can be seen, the behaviour of the breakthrough curves are not similar to those obtained for HNO_3 and HCl at this concentration, as the second curve does not shift to the right with respect to the first curve; on the contrary, it moves to the left, and the third curve is practically the same as the second curve. It is worth mentioning that, at the time of

conducting these studies with this regenerant at this concentration, it was observed that holes were generated in the carbon bed, which may be because, when using this concentration of NaOH, the regenerant-adsorbent contact was so aggressive that it caused the destruction of the structure of a large quantity of BCM, pulverizing it and reducing the carbon bed with the increasing desorption cycles; for this reason, it was decided not to carry out the studies at 1 and 0.01 M.

3.3 Results of data modelling of breakthrough curves for fluoride adsorption using BCM

Table 3 shows the design parameters obtained from the breakthrough curves using the Thomas Model, Numerical Integration and ANNs, as well as *MTZ*, to determine the breakthrough (t_r) and saturation (t_s) times, the total adsorption zone (Δ_t), the size of the mass transfer zone that the contaminant travelled (*MTZ*) and the delay factor (r_f), in order to know the speed at which the contaminant moved within the packed bed. These parameters, in general, depend on the type of adsorbate, the initial concentration and the operating conditions of the packed columns.

Specifically, for the breakthrough curves using HNO_3 0.1 M, it can be seen that the breakthrough time increases from 3.04 to 5.17 h from cycle 1 to 2, and from the third cycle it begins to decrease down to 0.03 h in the sixth cycle, thus corroborating the behaviour of the breakthrough curves. In addition, in the first two breakthrough curves, the lowest *MTZ* values were obtained and, from the third curve, they begin to increase, which confirms the behaviour of the breakthrough curves, since the literature mentions that, as the MTZ value increases, the performance of the adsorption process decreases (Nasr *et al.* 2011). Similarly, the delay factor increases from 17.38 to 26.46 from cycle 1 to 2, and begins to decrease from the third cycle down to 3.10 in the sixth cycle. These results are consistent with breakthrough curves, since they indicate that the adsorbate in the first two curves moves more slowly within the column, which prolongs its contact with the BCM, thus favouring *MTZ* in a better use. The Thomas Model was used to estimate the maximum adsorption capacity (q_o) of the packed bed. Table 3 shows that the maximum adsorption capacity increases from 3.92 to 5.34 mg/g from the first to the second adsorption, and, from the third adsorption, it starts decreasing down to 0.84 mg/g in the sixth adsorption. Likewise, the small value of the rate constant (K_{TH}) obtained in the second cycle indicates that fluorides are transported more slowly through the adsorbent, and the diffusion process between the adsorbate and the adsorbent is slower, prolonging the transport time and thereby increasing the adsorption capacity; i.e., the rate constant has an inverse relationship with the adsorption capacity (Dena 2007). Regarding the correlation coefficients, these varied between 0.9422 and 0.9896, which indicates that these correlations have a good fit to the experimental data of the breakthrough curves. Numerical Integration was used to determine the maximum adsorption capacity and to make a comparison with the Thomas Model with respect to the adjustment of the data. Like the Thomas Model, it is observed that the adsorption capacity increases from the first to the second breakthrough curve from 4.29 to 6.11 mg/g, and decreases from the third curve down to 2.00 mg/g in the sixth adsorption. Numerical Integration presents a better correlation coefficient in most cases, since the values fluctuate between 0.9897 and 0.9997. Regarding ANNs training, they satisfactorily correlated the breakthrough curves, mostly with respect to the Thomas Model and Numerical Integration, since they presented correlation coefficients greater than 0.9965. Therefore, ANNs are a predictive tool that describes the dynamic behaviour of a packed fixed-bed column. Several authors have used ANNs as a tool for the prediction of experimental data, obtaining good correlations (Aksu and Gönen 2006). Other regenerants and concentrations show a similar

Table 3 Estimated design parameters for the breakthrough curves using the Thomas Model, Numerical Integration, ANNs and MTZ in the adsorption-desorption process in a continuous system using HNO_3. HCl and NaOH as regenerants

	Cycle	Parameters of the packed fixed-bed column					ANNs	Parameters of the Thomas model			Numerical integration	
		t_r, h	t_s, h	Δ_t, H	MTZ, cm	r_f	R^2	K_{TH}, L/h mg	q_o, mg/g	R^2	q_{cal}, mg/g	R^2
HNO_3 1 M	1	3.40	64.77	61.36	7.11	9.84	0.9943	5.170E-03	3.11	0.9652	3.66	0.9964
	2	0.42	26.25	25.83	7.38	4.74	0.9957	1.202E-02	1.14	0.9603	2.04	0.9971
	3	0.01	23.33	23.33	7.50	5.10	0.9946	8.640E-03	1.05	0.9672	1.57	0.9758
HNO_3 0.1 M	1	3.04	61.44	58.40	7.13	17.38	0.9965	4.75E-03	3.92	0.9896	4.29	0.9995
	2	5.17	67.48	62.31	6.93	26.46	0.9965	4.53E-03	5.34	0.9830	6.11	0.9997
	3	2.44	67.62	65.18	7.23	15.11	0.9966	4.06E-03	3.44	0.9736	4.22	0.9974
	4	0.50	38.92	38.42	7.40	7.11	0.9971	7.26E-03	1.58	0.9711	2.54	0.9951
	5	0.03	67.79	67.76	7.50	3.00	0.9975	1.05E-02	0.85	0.9472	2.28	0.9941
	6	0.03	49.21	49.18	7.50	3.10	0.9977	1.17E-02	0.84	0.9422	2.00	0.9897
HNO_3 0.01 M	1	2.31	46.70	44.39	7.13	11.85	0.9966	1.08E-02	2.08	0.9871	3.67	0.9987
	2	0.72	45.00	44.28	7.38	7.70	0.9956	1.44E-02	1.35	0.9805	2.10	0.9982
	3	0.02	45.00	44.98	7.50	5.93	0.9968	1.06E-02	1.14	0.9683	2.50	0.9942
	4	0.02	55.00	54.98	7.50	3.56	0.9971	3.40E-03	1.62	0.9182	2.60	0.9872
	5	0.01	15.90	15.89	7.50	1.89	0.9870	4.12E-02	0.01	0.9687	2.12	0.9781
HCl 1 M	1	3.67	73.50	69.83	7.13	11.97	0.9943	4.01E-03	4.18	0.9575	4.79	0.9989
	2	3.12	28.97	25.85	6.69	12.80	0.9957	8.91E-03	2.48	0.9931	2.79	0.9985
	3	0.01	18.79	18.78	7.50	1.66	0.9946	2.57E-02	0.42	0.9537	1.45	0.9765
HCl 0.1 M	1	2.43	57.00	54.58	7.18	20.74	0.9973	4.54E-03	4.26	0.9925	4.37	0.9994
	2	1.10	61.00	59.90	7.38	41.47	0.9953	3.18E-03	7.56	0.9931	7.63	0.9993
	3	0.02	51.17	51.15	7.50	8.29	0.9966	7.79E-03	1.71	0.9705	2.91	0.9979
	4	0.02	47.17	47.15	7.50	5.93	0.9919	6.55E-03	1.54	0.9587	2.61	0.9978
	5	0.01	15.17	15.16	7.50	3.32	0.9954	4.32E-02	1.31	0.9442	2.23	0.9711
HCl 0.01 M	1	1.80	49.00	47.20	7.23	13.57	0.9970	7.12E-03	3.00	0.9854	3.60	0.9983
	2	0.03	45.17	45.14	7.50	3.56	0.9975	1.74E-02	0.74	0.9612	2.02	0.9968
	3	0.02	67.17	67.15	7.50	2.13	0.9976	2.92E-02	0.41	0.9482	1.72	0.9887
	4	0.02	60.00	59.98	7.50	2.37	0.9973	2.37E-02	0.47	0.9551	1.64	0.9852
NaOH 0.1 M	1	3.46	50.52	47.06	6.99	10.43	0.9934	9.56E-03	2.43	0.9866	3.20	0.9989
	2	0.47	37.29	36.82	7.41	9.44	0.9977	7.73E-03	1.72	0.9808	2.52	0.9981
	3	0.49	55.29	54.81	7.43	8.14	0.9970	1.09E-01	1.10	0.9794	2.40	0.9955

behaviour; in general, the breakthrough and saturation times and the delay factor decrease with increasing adsorption cycles. In addition, the MTZ values increase with the adsorption cycles, indicating a decrease in the performance of the adsorption process. Together with the Thomas Model and Numerical Integration, this confirms the behaviour of the breakthrough curves, since the adsorption capacity decreases and the K_{TH} value increases as the adsorption cycles increase. Regarding the ANNs, again, they presented a better adjustment to the breakthrough curves.

Table 4 Amount of desorbed milligrams of flourides in each cycle

Regenerant/concentration	Desorbed mg of fluorides/Cycle					
	1	2	3	4	5	6
HNO_3 0.1 M	13.63	6.37	6.72	19.58	26.37	26.21
HNO_3 0.01 M	13.62	25.46	28.39	23.83	12.73	
HNO_3 1 M	1.47	3.79	3.52			
HCl 0.1 M	4.80	5.63	6.50	12.29	21.46	
HCl 0.01 M	16.55	26.54	29.15	28.87		
HCl 1 M	1.47	3.79	3.52			
NaOH 0.1 M	4.41	4.82	3.54			

To sum up, when comparing the three concentrations of the regenerants HNO_3 and HCl, it is clear that the best results are obtained with 0.1 M, since, when adding the adsorption capacities of the first three cycles, 12.70, 4.57 and 5.30 mg/g are obtained for HNO_3 at 0.1, 0.01 and 1 M, respectively, for the Thomas Model, and 14.62, 8.27 and 7.27 mg/g are obtained at 0.1, 0.01 and 1 M, respectively, for Numerical Integration. For HCl, 13.53, 4.15 and 7.08 mg/g are obtained at 0.1, 0.01 and 1 M, respectively, for the Thomas Model, and 14.91, 7.34 and 9.03 mg/g are obtained at 0.1, 0.01 and 1 M, respectively, for Numerical Integration. Lastly, for NaOH at 0.1 M, 5.25 and 8.12 mg/g are obtained for the Thomas Model and Numerical Integration, respectively. It is important to mention that the values of the breakthrough and saturation times, the delay factor, *MTZ* and the rate constant K_{TH} confirm that 0.1 M is the best concentration.

3.4 BCM regeneration

In general, the fluoride desorption curves (See Fig. 12 and Table 4) show a similar behaviour: at the beginning of each study, a large amount of fluoride is desorbed, and, as time passes, it decreases until it remains almost constant. The tendency of each of these curves is to desorb more pollutant with the increasing desorption cycles, since the BCM in each adsorption cycle increases the amount of fluorides adsorbed. In the case of HNO_3 at 0.1 M, the study concluded with the completion of 6 adsorption-desorption cycles, since the behaviour was similar with each cycle, i.e., the breakthrough curve gradually shifted toward the y-axis, and the adsorption capacity at the last breakthrough curve was very low. Based on the modelling of the experimental data obtained by numerical integration from the desorption process, the amount of desorbed milligrams of fluorides in each cycle was calculated. From the first to the sixth cycle, 13.63, 6.37, 6.72, 19.58, 26.37 and 26.21 mg of fluorides were desorbed, respectively. It can be observed that, in the first three adsorption-desorption cycles, the desorbed amount of fluorides is low. This is due to the fact that the regenerant does not fully desorb the adsorbent material and, in each cycle, the quantity of fluorides adhered to said material remains constant. As the cycles increase, the amount of desorbed milligrams increases due to the saturation suffered by the adsorbent. With regard to HNO_3 at 0.01 M, the amount of desorbed milligrams of fluorides from the first to the fifth cycle was 13.62, 25.46, 28.39, 23.83 and 12.73 mg, respectively. Regarding at HNO_3 1 M, the amount of fluoride desorbed in the first, second and third cycle is 1.47 mg, 3.79 and 3.52 mg, respectively. With respect to HCl at 0.01 M, 16.55, 26.54, 29.15 and 28.87 mg of fluorides were desorbed in the first, second, third and fourth cycle, respectively. The tendency of the desorption process is similar when using HCl at

(1)

(2)

(3)

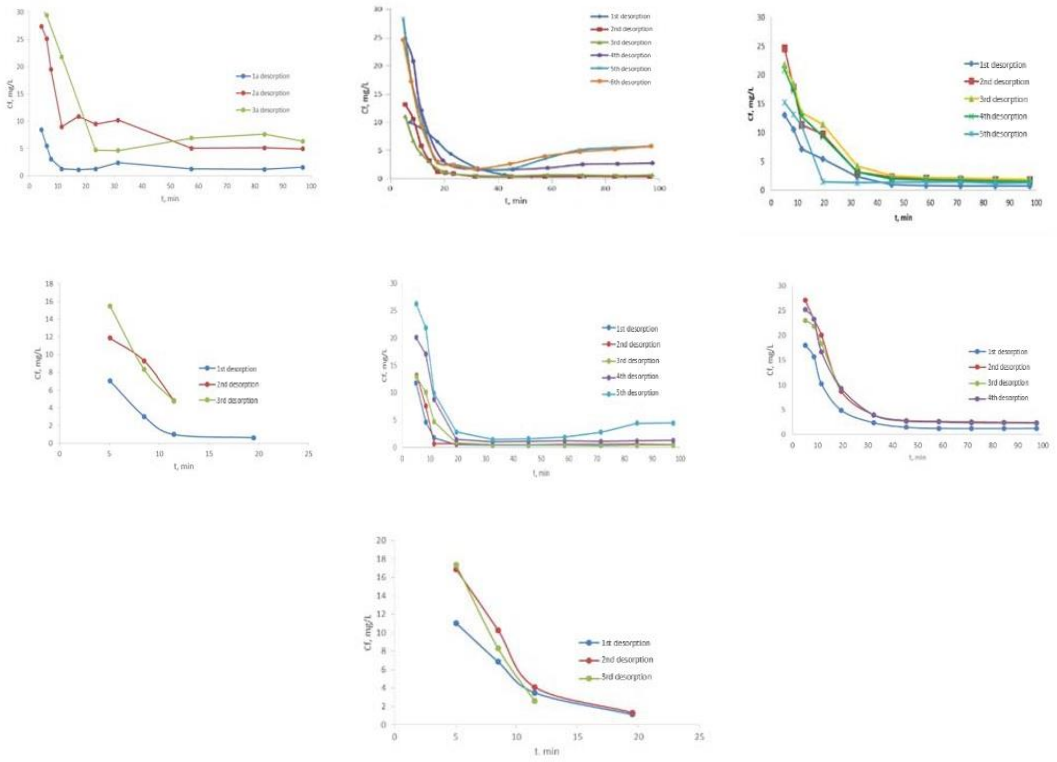

Fig. 12 Desorption curves of fluorides using: (1) HNO_3, (2) HCl, 3) NaOH at: (a) 1 M, (b) 0.1 M and (c) 0.01 M

0.1 M, since 4.80, 5.63, 6.50, 12.29 and 21.46 mg were desorbed in cycles 1 to 5, respectively. Lastly, in the case of HCl at 1 M, 3 cycles were obtained, in which 1.47, 3.79 and 3.52 mg of fluorides were desorbed. Therefore, by increasing the cycles, the amount of desorbed fluorides increases, due to the saturation of the adsorbent material, in addition to the fact that high concentrations of regenerant are aggressive for the adsorbent, as in the case of HCl 1 M, where only three adsorption-desorption cycles were obtained. The desorption curves using NaOH as regenerant at 0.1 M behave in a similar way as those obtained with HNO_3 and HCl, thus it was decided not to carry out the studies at 1 and 0.01 M. In addition, the estimated values in the desorption process through numerical integration corroborate the aforementioned, since 4.41, 4.82 and 3.54 mg of fluorides were desorbed in the first, second and third cycle, respectively.

4. Conclusions

The adsorption studies allowed determining the number of adsorption-desorption cycles of fluoride removal from water on BCM, which depended on the type of regenerant used and its concentration. The use of HNO_3 or HCl as regenerant at 0.1 M allowed obtaining the highest number of adsorption-desorption cycles, increasing the adsorption capacity of BCM in the first

three adsorption-desorption cycles, resulting in 12.70 and 14.62 mg/g for HNO_3 and 13.53 and 14.91 mg/g for HCl, determined with the Thomas Model and Numerical Integration, respectively. Thus, the use of the BCM is maximised, substantially decreasing the operating cost. These results are promising for use in fluoride adsorption-desorption studies with water from different wells in the city of Aguascalientes at a laboratory and pilot scale level. The increase in the adsorption capacity in the breakthrough curves when using HNO_3 at 0.1 M may be due to the fact that this regenerant oxidizes BCM, forming OH^- groups on its surface and thereby causing an increase in the ion exchange and in the adsorption capacity of the adsorbent. With respect to HCl at 0.1 M, active Cl^- sites are generated on the BCM surface, favouring ion exchange with fluorides and, consequently, adsorption. The Thomas Model, numerical integration and ANNs fit adequately to all the experimental data of the fluoride breakthrough curves and the parameters obtained allowed confirming their behaviour. ANNs obtained the highest correlation coefficients for all the breakthrough curves, with values between 0.9870 and 0.9977.

Acknowledgements

The authors acknowledge the financial support provided by CONACYT, TecNM/Instituto Tecnológico de Aguascalientes (Mexico) and Universidad de Extremadura and Junta de Extremadura/FEDER ref. GRU15123 (Spain).

References

Aguayo, V.I.A., Bonilla, P.A., Hernandez, M.V., Montes, M.M.A. and Reynel, A.H.E. (2011), "Batch and column studies of Zn^{2+} removal from aqueous solution using chicken feathers as sorbents", *Chem. Eng. J.*, **167**, 67-76. https://doi.org/10.1016/j.cej.2010.11.107.

Aksu, Z. and Gönen, F. (2006), "Binary biosorption of phenol and chromium (VI) onto immobilized activated sludge in a packed bed: prediction of kinetic parameters and breakthrough curves", *Sep. Purif. Technol.*, **29**, 205-216. https://doi.org/10.1016/j.seppur.2005.09.014.

Apiratikul, R. and Pavasant, P. (2008), "Batch and column studies of biosorption of heavy metals by Caulerpa lentillifera", *Bioresour. Technol.*, **99**, 2766-2777. https://doi.org/10.1016/j.biortech.2007.06.036.

Ayawei, N., Ebelegi, A.N. and Wankasi, D. (2017), "Modelling and interpretation of adsorption isotherms", *J. Chem.*, **2017**, 1-11. https://doi.org/10.1155/2017/3039817.

Basheer, I.A. and Hajmeer, M. (2000), "Artificial neural networks: fundamentals, computing, design and application", *J. Microbiol. Meth.*, **43**, 3-31. https://doi.org/10.1016/S0167-7012(00)00201-3.

Bennett, M.C. and Abram, J.C. (1967), "Adsorption from solution on the carbon and hydroxyapatite components of bone char", *J. Colloid Interface Sci.*, **23**, 513-521. https://doi.org/10.1016/0021-9797(67)90198-1.

Bhatnagar, A., Hogland, W., Marques, M. and Sillanpaa, M. (2013), "An overview of the modification methods of activated carbon for its water treatment applications", *Chem. Eng. J.*, **219**, 499-511. https://doi.org/10.1016/j.cej.2012.12.038.

Bravo, S.U.I., Rico, M.R. and Iglesias, S.G.A. (2002), "Improvement of the empiricism in the back equation of state via hybrid neural networks", *Ind. Eng. Chem. Res.*, **41**, 3705-3713. https://doi.org/10.1021/ie010773b.

Buamah, R., Oduro, C.A. and Sadik, M.H. (2016), "Fluoride removal from drinking water using regenerated aluminum oxide coated media", *J. Environ. Chem. Eng.*, **4,** 250-258. https://doi.org/10.1016/j.jece.2015.10.036.

Cavas, L., Karabay, Z., Alyuruk, H., Dogan, H. and Demir, G.K. (2011), "Thomas and artificial neural network models for the fixed-bed adsorption of methylene blue by a beach waste Posidonia oceanica (L.) dead leaves", *Chem. Eng. J.*, **171**, 557-562. https://doi.org/10.1016/j.cej.2011.04.030.

Choy, K.K.H. and McKay, G. (2005), "Sorption of cadmium, copper, and zinc ions onto bone char using Crank diffusion model", *Chemosphere*, **60**, 1141-1150. https://doi.org/10.1016/j.chemosphere.2004.12.041.

Choy, K.K.H., Ko, C.K., Cheung, C.W., Porter, J.F. and McKay, G. (2004), "Film and intraparticle mass transfer during the adsorption of metal ions onto bone char", *J. Colloid. Interf. Sci.*, **271**, 284-295. https://doi.org/10.1016/j.jcis.2003.12.015.

Das, N., Pattanaik, P. and Das, R. (2005), "Defluoridation of drinking water using activated titanium rich bauxite", *J. Colloid Interf. Sci.*, **292**, 1-10. https://doi.org/10.1016/j.jcis.2005.06.045.

Dena, A.J.A. (2007), Master´s Thesis, Instituto Tecnológico de Aguascalientes, México.

Diaz, B.F., Navarro, Q.A., Grijalva, M., Grimaldo, M., Loyola, R.J. and Ortiz, D. (1997), "Endemic Fluorosis in México, *Fluoride*, **30**, 233-239.

Dimovic´, S., Smicˇiklas, I., Pleac´as, I., Antonovic´, D. and Mitric´, M. (2009), "Comparative study of differently treated animal bones for Co^{2+} removal", *J. Hazard. Mater.*, **164**, 279-287. https://doi.org/10.1016/j.jhazmat.2008.08.013.

Dubey, S., Agarwal, M. and Gupta, A.B. (2021), "Fluoride removal using Alum & PACl in batch & continuous mode with subsequent microfiltration", *Membr. Water Treat.*, **12**, 83-93. https://doi.org/10.12989/mwt.2021.12.2.083.

Faur, C., Cogunaud, A., Dreyfus, G., Cloirec, P.L. (2008), "Modelling the breakthrough of activated carbon filters by pesticides in surface waters with static and recurrent neural networks", *Chem. Eng. J.*, **145**, 7–15. https://doi.org/10.1016/j.cej.2008.02.015.

Fawell, J., Bailey, K., Chilton, J., Dahi, E., Fewtrell, L., Magara, Y. (2006), "Fluoride in drinking water, World Health Organization (WHO), IWA Publishing, London, UK., 2-134.

Gong, J.L., Zhang, Y.L., Jiang, Y., Zeng, G.M., Cuia, Z.H., Liu, K., Deng, C.H., Niu, Q.Y., Deng, J.H. and Huan, Sh.Y. (2014), "Continuous adsorption of Pb (II) and methylene blue by engineered graphite oxide coated sand in fixed-bed column", *Appl. Surf. Sci.*, **330**, 148-157. https://doi.org/10.1016/j.apsusc.2014.11.068.

Gupta, V.K., Ali, I. and Saini, V.K. (2007), "Defluoridation of wastewaters using waste carbon slurry", *Water Res.*, **41**, 3307-3316. https://doi.org/10.1016/j.watres.2007.04.029.

Ghorai, S. and Pant, K.K. (2005), "Equilibrium, kinetics and breakthrough studies for adsorption of fluoride on activated alumina", *Sep. Purif. Technol.*, **42**, 265-271. https://doi.org/10.1016/j.seppur.2004.09.001.

Han, R., Wang, Y., Zou, W., Wang, Y. and Shi, Y. (2007), "Comparison of linear and nonlinear analysis in estimating the Thomas model parameters for methylene blue adsorption onto natural zeolite in fixed-bed column", *J. Hazard. Mater.* **145**, 331–335. https://doi.org/10.1016/j.jhazmat.2006.12.027.

Han, R., Wang, Y., Zhao, X., Wang, Y., Xie, F., Cheng, F., Tang, M. (2009), "Adsorption of methylene blue by phoenix tree leaf powder in a fixed-bed column: experiments and prediction of breakthrough curves", *Desalination*. **245,** 284–297. https://doi.org/10.1016/j.desal.2008.07.013.

Hernández-Eudave, M.T., Bonilla-Petriciolet, A., Moreno-Virgen, M.R., Rojas-Mayorga, C.K. and Tovar-Gómez, R. (2016), "Design analysis of fixed-bed synergic adsorption of heavy metals and acid blue 25 on activated carbon", *Desalination Water Treat.*, **57**, 9824-9836. http://dx.doi.org/10.1080/19443994.2015.1031710.

Hernández, M.V., Bueno, L.J.I., Sánchez, R.A.M., García, S.J., Trejo, V.R, Bonilla, P.A. and Márquez, A.C. (2003), "Fluorosis and dental caries in children 9-11 years of age from the state of Aguascalientes, Mexico", *Rev. Int. Contam. Ambient.*, **19**, 197-204.

Hernández, M.V., Elizalde, G.M.P. and Trejo, V.R. (2007), "Screening of commercial sorbents for removal of fluoride in synthetic and groundwater", *Environ. Technol.*, **28**, 595-607. https://doi.org/10.1080/09593332808618823.

Hernández, M.V., Ramírez, M.L.A., Bonilla, P.A. and Montes, M.M.A. (2012), "Optimizing the removal of fluoride form water using new carbons obtained by modification of nut shell with a calcium solution from egg shell", *Biochem. Eng. J.*, **62**, 1-7. https://doi.org/10.1016/j.bej.2011.12.011.

Hosseine, S.S. and Denayer, J.F.M. (2022), "Biogas upgrading by adsorption processes: Mathematical modeling, simulation and optimization approach – A review", *J. Environ. Chem. Eng.*, **10**, 1-25. https://doi.org/10.1016/j.jece.2022.107483.

Kalavathy, H., Karthik, B. and Miranda, L.R. (2010), "Removal and recovery of Ni and Zn from aqueous solution using activated carbon from Hevea brasiliensis: Batch and column studies", *Colloids Surf. B: Biointerfaces*, **78**, 291-302. https://doi.org/10.1016/j.colsurfb.2010.03.014.

Kyzas, G.A., Siafaka, P.I., Pavlidou, E.G., Chrissafis, K.J. and Bikiaris, D.N. (2015), "Synthesis and adsorption application of succinyl-grafted chitosan for the simultaneous removal of zinc and cationic dye from binary hazardous mixtures", *Chem. Eng. J.*, **259,** 438-448. https://doi.org/10.1016/j.cej.2014.08.019.

Leyva-Ramos, R., Rivera-Utrilla, J., Medellin-Castillo, N.A. and Sanchez-Polo, M., (2010), "Kinetic modeling of fluoride adsorption from aqueous solution onto bone char", *Chem. Eng. J.*, **158**, 458-467. https://doi.org/10.1016/j.cej.2010.01.019.

Louadj, A., Bouras, O., Rebahie, I., Cheknane, O. and Zermane, F. (2021), "Study on dynamic adsorption and chemical regeneration of Cd(II) from textile effluents by new granular composite based on gluten", *Membr. Water Treat.*, **10**, 117-131. https://doi.org/10.12989/aer.2021.10.2.117.

Millar, G., Couperthwaite, S., Dawes, L., Thompson, S. and Spencer, J. (2017), "Activated alumina for the removal of fluoride ions from high alkalinity groundwater: New insights from equilibrium and column studies with multicomponente solutions", *Sep. Pur. Technol.*, **187**, 14-24. https://doi.org/10.1016/j.seppur.2017.06.042.

Nasr, A.B., Walha, K., Charcosset, C. and Amar, R.B. (2011), "Removal of fluoride ions using cuttlefish bones", *J. Fluorine Chem.*, **132**, 57-62. https://doi.org/10.1016/j.jfluchem.2010.11.006.

O´Connell, D.W., Birkinshaw, C. and O´Dwyer, T.F. (2008), "Heavy metal adsorbents prepared from the modification of cellolose, A review", *Bio Technol.*, **99**, 6703-6724. https://doi.org/10.1016/j.biortech.2008.01.036.

Oguz, E. and Ersoy, M. (2010), "Removal of Cu^{2+} from aqueous solution by adsorption in a fixed bed column and neural network modelling", *Chem. Eng. J.*, **164**, 56-62. https://doi.org/10.1016/j.cej.2010.08.016.

Öztürk, N., Yazar, M., Gündoğdu, A., Duran, C., Şentürk, H.B. and Soylak, M. (2021), "Application of cherry laurel seeds activated carbon as a new adsorbent for Cr(VI) removal", *Membr. Water Treat.*, **12**, 11-21. https://doi.org/10.12989/mwt.2021.12.1.011.

Omidvar, B.M., Pirsaheb, M., Vosoughi, N.M., Khosravi, M.R., Kakavandi, B., Reza, Z.M. and Asadi, A. (2016), "Batch and column studies for the adsorption of chromium (VI) on low-cost Hibiscus Cannabinus kenaf, a green adsorbent", *J. Taiwan Inst. Chem. Eng.*, **68**, 80-89. https://doi.org/10.1016/j.jtice.2016.09.022.

Pan, X., Wang, J. and Zhang, D. (2009), "Sorption of cobalt to bone char: kinetics, competitive sorption and mechanism", *Desalination*, **249**, 609-614. https://doi.org/10.1016/j.desal.2009.01.027.

Patel, H., Vashi, R.T. (2015), "Characterization and Treatment of Textile Wastewater", *Elsevier Inc.* 127-145. https://doi.org/10.1016/B978-0-12-802326-6.00006-X.

Rao, S.M., Reddy, B.V.V., Lakshmikanth, S. and Ambika, N.S. (2009), "Re-use of fluoride contaminated bone char sludge in concrete", *J. Hazard. Mater.*, **166**, 751-756. https://doi.org/10.1016/j.jhazmat.2008.11.115.

Rojas-Mayorga, C.K., Bonilla-Petriciolet, A., Aguayo-Villarreal, I.A., Hernández-Montoya, V., Moreno-Virgen, M.R., Tovar-Gómez, R. and Montes-Morán, M.A. (2013), "Optimization of pyrolysis conditions and adsorption properties of bone char for fluoride removal from water", *J. Anal. Appl. Pyrol.*, **104,** 10-18. http://dx.doi.org/10.1016/j.jaap.2013.09.018.

Singh, S., Ashfaq, M., Kumar, S.R., Joshi, H.C., Srivastava, A., Sharma, A. and Verma, N. (2013), "Preparation of surfactant-mediated silver and copper nanoparticles dispersed in hierarchical carbon

micro-nanofibers for antibacterial applications", *New Biotechnol.*, **30**, 656-665. https://doi.org/10.1016/j.nbt.2013.05.002.

Standard Methods for Examination of Water and Wastewater, American Public Health Association, 20th Ed., (1998).

Susheela, A.K., Taposh, K. and Das, K. (1992), "Fluoride ingestion and its correlation with gastrointestinal discomfort", *Fluoride*, **25**, 5-22.

Texier, A.C., Andrés, Y., Faur-Brasquet, C. and Cloirec, P.L., (2002), "Fixed-bed study for lanthanide (La, Eu, Yb) ions removal from aqueous solutions by immobilized Pseudomonas aeruginosa: experimental data and modelization", *Chemosphere*, **47,** 333-342. https://doi.org/10.1016/S0045-6535(01)00244-2.

Thomas, H.C. (1944), "Heterogeneous ion exchange in a flowing system", *J. Am. Chem. Soc*., **66**, 1664-1666. https://doi.org/10.1021/ja01238a017.

Tovar G.R., Moreno, V.M.R., Dena, A.J.A., Hernández, M.V., Bonilla, P.A. and Montes, M.M.A. (2013), "Modeling of fixed-bed adsorption of fluoride on bone char using a hybrid neural network approach", *Chem. Eng. J*., **228**, 1098-1109. http://dx.doi.org/10.1016/j.cej.2013.05.080.

Yiamouyiannis, J. and Burk, D. (1997), "Fluoridation and cancer, age-dependence of cancer mortality related to artificial fluoridation", *Fluoride*, **10**, 102-124.

Yoon, Y.H. and Nelson, J.H. (1984), "Application of gas adsorption kinetics I. A theoretical model for respirator Cartridge service life", *Am. Ind. Hyg. Assoc. J*., **45,** 509-516. https://doi.org/10.1080/15298668491400197.

Yu, J., Zhu, J., Feng, L., Cai, X., Zhang, Y. and Chi, R. (2014), "Removal of cationic dyes by modified waste biosorbent under continuous model: competitive adsorption and kinetics", *Arab. J. Chem*., **12**, 2044-2051. https://doi.org/10.1016/j.arabjc.2014.12.022.

Zhu, T., Zhu, T., Gao, J., Zhang, L., Zhang, W. (2017), "Enhanced adsorption of fluoride by cerium immobilized cross-linked chitosan composite", *J Fluorine Chem.*, **194**, 80-88. https://doi.org/10.1016/j.jfluchem.2017.01.002.

CC